Computer Coupling of Phase Diagrams and Thermochemistry 32 (2008) 543–565

Contents lists available at ScienceDirect

Computer Coupling of Phase Diagrams and Thermochemistry

journal homepage: www.elsevier.com/locate/calphad

First-principles based calculation of binary and multicomponent phase diagrams for titanium carbonitride

D.A. Andersson [a,*], P.A. Korzhavyi [a], B. Johansson [a,b]

[a] Applied Materials Physics, Department of Materials Science and Engineering, Royal Institute of Technology, SE-100 44 Stockholm, Sweden

[b] Condensed Matter Theory Group, Department of Physics, Uppsala University, Box 530, SE-751 21 Uppsala, Sweden

ARTICLE INFO

Article history:
Received 1 March 2007
Received in revised form
17 April 2008
Accepted 27 April 2008
Available online 9 June 2008

Keywords:
First-principles calculations
CALPHAD
Titanium carbonitride
Order–disorder reactions
Phase diagrams

ABSTRACT

In this paper we have used a combined first principles and Calphad approach to calculate phase diagrams in the titanium–carbon–nitrogen system, with particular focus on the vacancy-induced ordering of the substoichiometric carbonitride phase, TiC_xN_y ($x+y \leq 1$). Results from earlier Monte Carlo simulations of the low-temperature binary phase diagrams are used in order to formulate sublattice models for TiC_xN_y within the compound energy formalism (CEF) that are capable of describing both the low temperature ordered and the high-temperature disordered state. We parameterize these models using first-principles calculations and then we demonstrate how they can be merged with thermodynamic descriptions of the remaining Ti–C–N phases that are derived within the Calphad method by fitting model parameters to experimental data. We also discuss structural and electronic properties of the ordered end-member compounds, as well as short range order effects in the TiC_xN_y phase.

1. Introduction

Theoretical phase diagram calculations can be divided into two main categories; empirical (phenomenological) methods and first-principles methods. The so-called Calphad method [1,2] is an example of the first approach, in which models for the thermodynamic properties of each phase, i.e. Gibbs free energy, are fitted to experimental information in a procedure called assessment.

The Calphad method can be made less dependent on performing new experiments by incorporating data from first-principles calculations, which are only based on quantum mechanics (first-principles or *ab initio* calculations) and statistical mechanics (Monte Carlo, etc.) [3–5], into the assessment procedure. This task is not necessarily straightforward since there are several cases where first-principles calculations and experiments are known to disagree quite significantly [6]. Consistent results are needed in order to build compatible thermodynamic models. Difficulties also arise from the need to treat finite temperature properties, which are not directly accessible from first-principles calculations, especially when the compounds are dynamically unstable [7,8]. The formalism of how to apply first-principles calculations in a consistent way has been discussed in Refs. [6,9,10]. Existing examples of combined Calphad and ab-initio approaches include [12–20]. The present paper deals with modeling of phase equilibria in titanium carbonitride, TiC_xN_y ($x + y \leq 1$), starting from first-principles calculations. The carbonitride phase, hereafter denoted as δ, crystallizes in the cubic B1 (NaCl) structure. In the absence of dissolved oxygen δ-TiC_xN_y does not contain any vacancies on the metallic sublattice (Ti), whereas the nonmetal sublattice may incorporate a great amount of structural vacancies (in which case $x+y < 1$) [11]. Our prime interest is to describe and model the substoichiometry due to nonmetal vacancies. The reason for our interest in TiC_xN_y is its unique set of properties, e.g. high chemical stability, great hardness, high melting point and excellent thermal conductivity, which makes it useful for technological applications, for instance as coating material in cutting tools [21]. We use first-principles calculations together with results from earlier Monte Carlo simulations [22,23] to derive models of Calphad type for δ-TiC_xN_y and to estimate model parameters that in many cases would be impossible to obtain from experiments.

This paper is organized as follows. First we discuss the current theoretical and experimental understanding of δ-TiC_xN_y, as well as the relevant phase equilibria in the Ti–C–N system. The details of our first-principles calculations and the thermodynamic models for all the Ti–C–N phases are described in Section 3. In Section 4 we present and discuss our results. Finally, we summarize our findings in Section 5. The database derived in this work contains too much data to be convenient to publish in printed form, we therefore encourage interested readers to contact the authors or visit

* Corresponding author.
E-mail address: davida@mse.kth.se (D.A. Andersson).

0364-5916/$ – see front matter © 2008 Elsevier Ltd. All rights reserved.
doi:10.1016/j.calphad.2008.04.007

Table 1
Basis vectors (native coordinates $\chi\eta\zeta$) of the sublattice sites in the $\{111\}_{B1}$ stacking model presented in Fig. 2

Atom	χ	η	ζ	Subl.	Atom	χ	η	ζ	Subl.
C 1	0	0	0	1	Ti 1	1/3	5/12	1/4	7
C 2	1/3	2/3	0	2	Ti 2	2/3	1/12	1/4	7
C 3	2/3	1/3	0	3	Ti 3	0	3/4	1/4	7
C 4	2/3	5/6	1/2	4	Ti 4	1/3	11/12	3/4	7
C 5	1/3	1/6	1/2	5	Ti 5	0	1/4	3/4	7
C 6	0	1/2	1/2	6	Ti 6	2/3	7/12	3/4	7

The 'Subl.' column specifies the sublattice number in the six-sublattice model, which is described in Section 3.2.7.

www.mse.kth.se/projects/cct/cct.html to obtain the parameter set in electronic format.

2. Existing models and experiments

2.1. Titanium carbide, Ti–C

Jonsson [24], Seifert et al. [25], Dumitrescu et al. [26] and Frisk [27] have presented Calphad assessments of the Ti–C system. In these works the δ phase is treated as a solution phase and modeled with a two-sublattice model, $(Ti)_1(C, Va)_1$, where Ti completely occupies one sublattice and C partially occupies the other, thus leaving vacancies. Carbon and vacancies form a solid solution on the second sublattice and any ordering at low temperature is ignored in the model. Fig. 1 shows the phase diagram from the most recent assessment by Frisk [27]. For an extensive review of the experimental thermodynamic data and phase equilibria in the Ti–C system we refer the reader to Refs. [24,26]. Both α-Ti (HCP) and β-Ti (BCC) have low solubility of carbon. At low carbon content the δ-TiC_x phase boundary is quite steep, which hints that the phase field is limited by the formation of an almost stoichiometric (fixed composition) compound. From experiments [28] the δ phase is known to order below ≈1000 °C, both cubic and trigonal forms of the Ti_2C compound have been observed [28–31]. Refs. [32,33] identified cubic and trigonal Ti_2C superstructures as well as a rhombohedral Ti_3C_2 phase. The existence of a Ti_3C_2 superstructure is also consistent with the diffuse neutron diffraction maxima observed in $TiC_{0.61}$ at 600 °C [22,28]. The stability of Ti_2C, Ti_3C_2 and Ti_6C_5 superstructures have been confirmed by extensive theoretical calculations using the cluster expansion technique, the generalized perturbation method, and Monte Carlo simulations [22]. The ordering temperatures reported by Korzhavyi et al. [22] agree well with available experimental transition temperatures. Diffusion is very sluggish in δ-TiC_x and long annealing times are required to reach the low-temperature equilibrium state, which makes an experimental exploration of this part of the phase diagram difficult. According to Korzhavyi et al. [22] the ordering of carbon vacancies in TiC_x can be rationalized in terms of filled, partially filled and empty $\{111\}_{B1}$ nonmetal planes. Within the $\{111\}_{B1}$ nonmetal planes vacancies and carbon atoms arrange in a hexagonal pattern. This stacking and the in-plane ordering is illustrated in Fig. 2. The ordering patterns reflect the tendency of carbon vacancies to avoid the NN (nearest neighbor) and 2NN (second nearest neighbor) positions, but instead favor the 3NN and 4NN (third and fourth nearest neighbor) positions [22]. Stacking of the partially filled $\{111\}_{B1}$ planes may occur along the $[1, 1/2, 1/2]_{B1}$, $[1/2, 1, 1/2]_{B1}$ and $[1/2, 1/2, 1]_{B1}$ directions (also 3NN vectors). Different stacking sequences produce different symmetries [22]. In the simplest case the stacking is linear along one of the stacking directions. All the possible stacking sequences are close in energy [22], thus for studying the energetics it is sufficient to consider the simplest linear stacking scheme. By splitting (at least) one of the nonmetal $\{111\}_{B1}$ planes into two or more sublattices, it is possible to describe the Ti_2C, Ti_3C_2 and Ti_6C_5 superstructures within one common sublattice model. The corresponding unit cell is monoclinic and it contains two nonmetal and two metal $\{111\}_{B1}$ planes with 12 sites in total (Fig. 2). The lattice coordinates are summarized in Table 1. By construction this unit cell serves as basis for a sublattice model of δ-TiC_x that is capable of describing the low-temperature ordered phases, as well as the high-temperature disordered state. In Section 4.1.1 we use first-principles calculations to estimate the phase stability of the ordered TiC_x structures that can be formed from the sublattice model and in Section 4.3.1 we apply the sublattice model to predict phase equilibria. For the Ti_2C composition there is an ordered phase with cubic symmetry [22,34] that is marginally more stable than the trigonal structure modeled with the unit cell in Fig. 2.

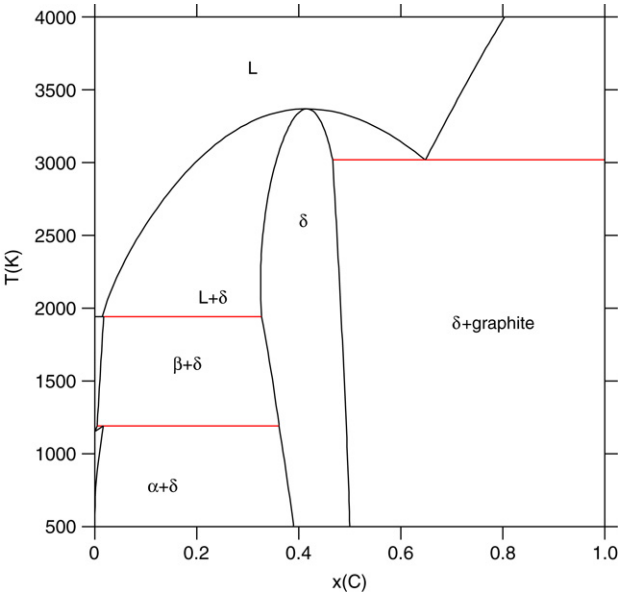

Fig. 1. The Ti–C phase diagram calculated with the parameter set in Ref. [27].

2.2. Titanium nitride, Ti–N

The two most recent Calphad assessments of the Ti–N system are due to Jonsson [35] and Zeng et al. [36]. For a review of the experimental thermodynamic data we refer to Jonsson [35]. The assessed Ti–N phase diagram is shown in Fig. 3. Compared to the Ti–C phase diagram in Fig. 1, both the α-Ti and β-Ti phases dissolve much more nitrogen than carbon. The δ-TiN_x phase is similar to the δ-TiC_x phase and δ-TiN_x is usually modeled in the same way as the carbide phase. The δ-TiN_x phase field is wider than the phase field of δ-TiC_x and, moreover, an ordered phase, ϵ-Ti_2N, having the anti-rutile structure [37,38] appears at low temperature. There is also an ordered δ-Ti_2N phase that is directly related to the vacancy containing cubic B1 structure [31] (not shown in Fig. 3). Lengauer [39] reported ordered hexagonal phases with the Ti_4N_3 and Ti_3N_2 stoichiometries, however these have a limited stability range and will not be considered in the present work. Using cluster expansion techniques Hart et al. [23] calculated the ground-state

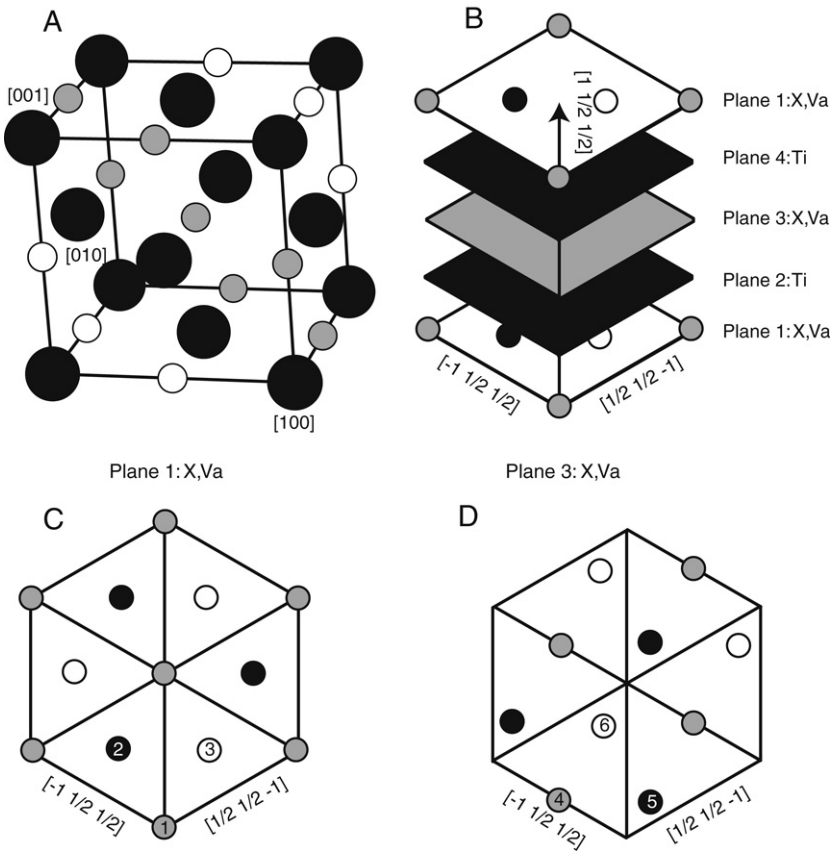

Fig. 2. The stacking of filled, partially filled and empty $\{111\}_{B1}$ planes in TiC_x. The lattice coordinates are given in Table 1. (A) The underlying B1 structure with the $\{111\}_{B1}$ planes highlighted. The Ti sites are shown in black and the nonmetal sites in white (plane 1) or in grey (plane 3). (B) The stacking of the $\{111\}_{B1}$ planes. Only the nonmetal sites are shown. (C) The hexagonal ordering in the first nonmetal plane. The numbers refer to the different sublattices. (D) The hexagonal ordering in the second nonmetal plane. The numbers refer to the different sublattices.

structures of vacancy ordered TiN_x. Specifically, they found stable superstructures with the Ti_2N, Ti_3N_2 and Ti_6N_5 stoichiometries. According to their results these structures are made up of filled and half-filled $\{011\}_{B1}$ planes stacked on top of each other. This vacancy ordering is somewhat different from the $\{111\}_{B1}$ TiC_x stacking, especially around the Ti_2N composition, which reflects the fact that the vacancy–vacancy interactions are not the same in the carbide and nitride systems. For example, the 2NN vacancy repulsion is much stronger for carbon vacancies than for nitrogen vacancies (see Section 4.3.2). The lowest-energy δ-Ti_2N superstructure found by Hart et al. [23] has half-filled $\{011\}_{B1}$ nonmetal planes and it is identical to the ordered structure reported in Ref. [31]. The $\{011\}_{B1}$ stacking can be modeled with a unit cell of 24 sites, which in total contains 12 $\{011\}_{B1}$ lattice planes with two sites per plane. The stacking direction is $[1\ 0\ 2]_{B1}$. The vacancy ordered structures can be described by splitting the nonmetal planes into two different sublattices. The unit cell and the different sublattices are depicted in Fig. 4 and Table 2 contains all the lattice coordinates. Closer inspection of the $\{111\}_{B1}$ and $\{011\}_{B1}$ stacking models reveals that the Ti_6X_5 (X is C or N) superstructures are almost identical in the two structure models. The properties of the ordered TiN_x vacancy structures formed from the $\{011\}_{B1}$ sublattice model are studied in Section 4.1.2 and in Section 4.3.2 we apply this model to predict phase equilibria.

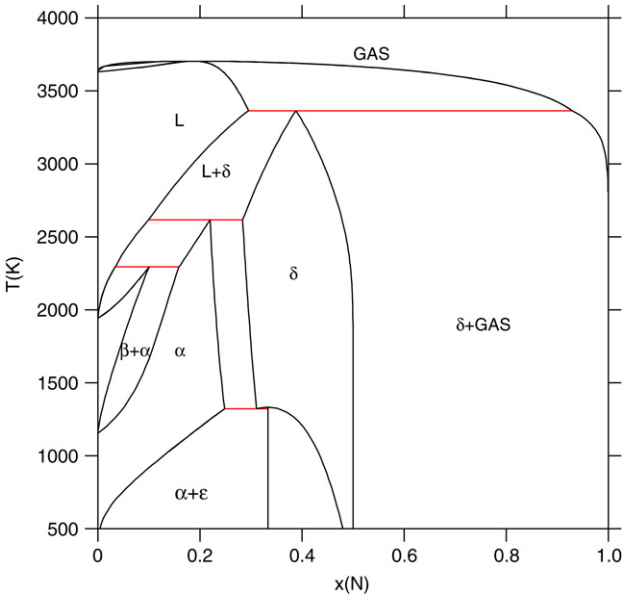

Fig. 3. The Ti–N phase diagram calculated with the parameter set in Ref. [35].

2.3. Titanium carbonitride, Ti–C–N

The ternary Ti–C–N system was recently assessed by Frisk et al. [41], who used the works of Jonsson [40] and Dumitrescu et al. [26] as starting points. Refs. [26,40] contain comprehensive compilations of available experimental thermodynamic data. Fig. 5 shows a constant temperature section at 1423 K of the Ti–C–N phase diagram and it was obtained with the parameter set from Frisk et al. [41]. None of the existing assessments treat any ordering reactions in the δ-TiC_xN_y phase at low temperature, thus

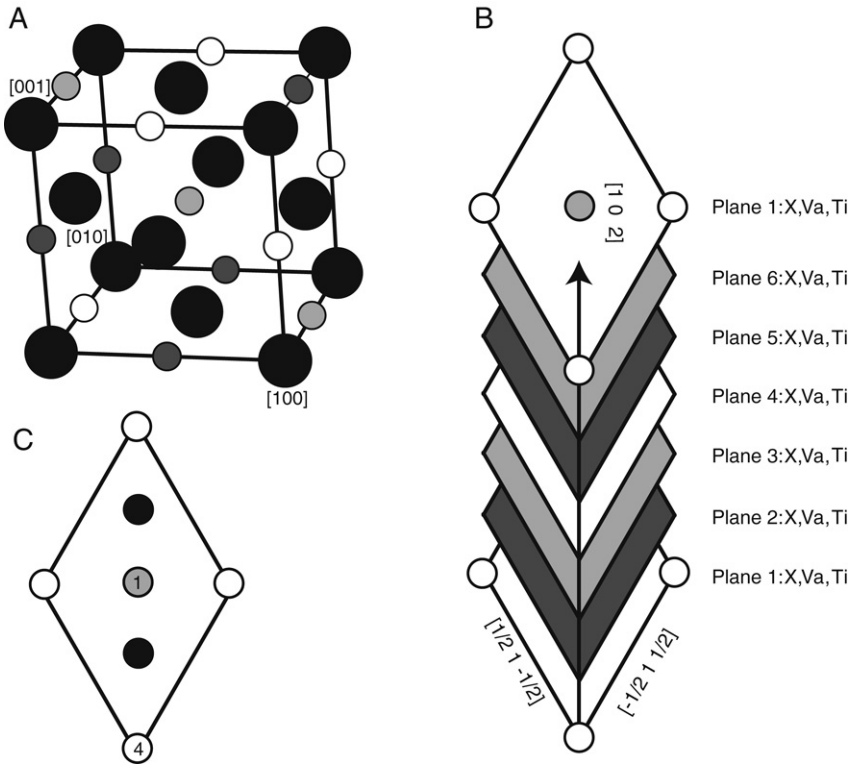

Fig. 4. The unit cell and the different sublattices of the $\{011\}_{B1}$ stacking model of TiN_x. The lattice coordinates are given in Table 2. Each $\{011\}_{B1}$ plane contains both Ti and nonmetal sites. (A) The underlying B1 structure with the different $\{011\}_{B1}$ planes highlighted. The Ti sites are shown in black and the nonmetal sites in white (plane 1 and 4), in dark grey (plane 2 and 5) or in light grey (plane 3 and 6). (B) The stacking of the $\{011\}_{B1}$ planes. Only the nonmetal sites are shown in plane 1. (C) The ordering in the first $\{011\}_{B1}$ plane. The symmetry is the same in the other $\{011\}_{B1}$ planes, but the atomic positions are shifted in relation to the unit cell boundaries. The numbers refer to the different sublattices and the black dots are Ti sites.

Table 2
Basis vectors (native coordinates $\chi\eta\zeta$) of the sublattice sites in the $\{011\}_{B1}$ stacking model presented in Fig. 4

Atom	χ	η	ζ	Subl.	Atom	χ	η	ζ	Subl.
N 1	1/2	1/2	0	1	Ti 1	7/12	11/12	2/3	7
N 2	1/4	1/4	1/2	1	Ti 2	1/6	5/6	5/6	7
N 3	7/12	11/12	1/6	2	Ti 3	11/12	7/12	1/3	7
N 4	5/6	1/6	2/3	2	Ti 4	1/2	1/2	1/2	7
N 5	1/6	5/6	1/3	3	Ti 5	1/12	5/12	2/3	7
N 6	11/12	7/12	5/6	3	Ti 6	2/3	1/3	11/12	7
N 7	0	0	0	4	Ti 7	1/4	1/4	0	7
N 8	3/4	3/4	1/2	4	Ti 8	0	0	1/2	7
N 9	1/12	5/12	1/6	5	Ti 9	5/12	1/12	1/3	7
N 10	1/3	2/3	2/3	5	Ti 10	3/4	3/4	0	7
N 11	2/3	1/3	1/3	6	Ti 11	5/6	1/6	1/6	7
N 12	5/12	1/12	5/6	6	Ti 12	1/3	2/3	1/6	7

The 'Subl.' column specifies the sublattice number in the six-sublattice model, which is described in Section 3.2.7.

it is not possible to study how the $\{011\}_{B1}$ (TiN_y) and $\{111\}_{B1}$ (TiC_x) stacking of vacancies merge in the ternary phase field. There is limited experimental information about ternary ordered phases, though some early data were reported by Arbuzov [42]. By extending the binary sublattice models to the ternary case, i.e. by allowing both carbon and nitrogen to occupy the nonmetal sublattices, we investigate the properties of the ternary δ-TiC_xN_y compounds and the ternary phase diagram in Section 4.2 and Section 4.3.3, respectively.

3. Theoretical background

3.1. First-principles calculations

The first-principles total-energy calculations were performed with the frozen-core all electron projector augmented wave (PAW) method, as implemented in the *ab initio* total-energy and molecular-dynamics program VASP (Vienna *ab-initio* simulation package) [43–47]. The semi-core Ti-3s and Ti-3p states were kept frozen. Including these states among the valence electrons only resulted in minor changes for the properties of present interest. The exchange and correlation effects were treated with the generalized gradient approximation (GGA) [48], since this parameterization is known to give an accurate description of both TiC and TiN [49]. The equilibrium volume of every structure was determined by optimizing all internal structural parameters, i.e. both the shape of the unit cell and the atomic positions, at constant cell volume and then minimizing the energy by performing the same procedure at several cell volumes around the equilibrium. The internal structural parameters were relaxed until the Hellman–Feynman forces on each ion were negligible ($<$0.01 eV/Å). By fitting the calculated total energies

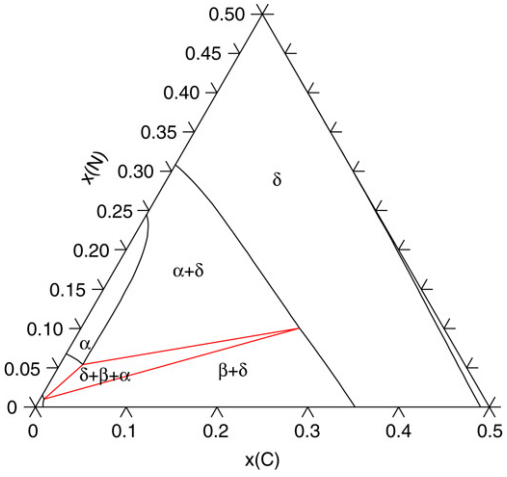

Fig. 5. The Ti–C–N phase diagram at 1423 K calculated with the parameter set in Ref. [41].

to the Murnaghan equation of state [50] we obtained the pressure–volume relation and an estimate of the bulk modulus (B) as well as of its pressure derivative (B'). The convergence with respect to the k-point mesh and the cut-off energy for the plane wave basis set were carefully checked. We used a cut-off energy of 400 eV for all our calculations. Monkhorst–Pack $8 \times 8 \times 8$ k-point meshes [51] were used for both the $\{111\}_{B1}$ and $\{011\}_{B1}$ stacking sequence unit cells, which correspond to 256 and 90 irreducible k points, respectively. The Brillouin-zone integration was performed using the Methfessel–Paxton smearing with a smearing parameter of 0.20 eV. The electronic density of states (DOS) was obtained with $11 \times 11 \times 11$ k-point meshes for both the $\{111\}_{B1}$ and the $\{011\}_{B1}$ stacking sequence unit cells (366 irreducible k-points for the $\{111\}_{B1}$ stacking sequence unit cell and 216 for the $\{011\}_{B1}$ stacking sequence unit cell) together with the linear tetrahedron method with Blöchl corrections [52].

In order to estimate the relative phase stability of nonstoichiometric carbides and nitrides we need to establish the reference energies of Ti, C and N. For reasons of compatibility with existing thermodynamic databases we use α-Ti, graphite and the N_2 molecule as reference states. The energies of α-Ti and N_2 are rather straightforward to calculate with density functional schemes, however this is not the case for graphite. Graphite is built up from hexagonal sheets of carbon atoms. Within these sheets the carbon atoms are covalently bonded, but the bonding between the sheets is of long-range van der Waals type, which is not well described by any of the standard approximations for the exchange-correlation effects [53]. To overcome this problem we calculated the total energy of carbon in the diamond structure and then we used the assessed heat of transformation between the diamond and graphite structures [54] to estimate the stability of graphite. The formation energy of TiC_xN_y is defined as

$$H_f = (H(TiC_xN_y) - H(\alpha\text{-Ti}) - xH(\text{C, Graphite}) - \frac{y}{2}H(N_2, \text{Gas}))/(1+x+y). \quad (1)$$

Here $H(TiC_xN_y)$ is the fully relaxed energy of TiC_xN_y, $H(\alpha$-Ti) is the energy of titanium in its ground-state hexagonal close-packed structure, and $H(N_2, \text{Gas})$ is the energy of a nitrogen molecule.

3.2. Calphad modeling

We will use the compound energy formalism (CEF) to model Gibbs free energy of the binary and ternary Ti–C–N solution phases [55]. The model parameters of the δ phase are derived solely from first-principles calculations, but for the other phases, i.e. the α-Ti, β-Ti, liquid (L) and gas phases, we rely on experimental data. Below we describe the CEF models in detail. The thermodynamic models have been implemented using the Thermo-Calc software [56].

3.2.1. α-Ti

Dissolution of carbon and nitrogen in α-Ti is modeled with a two-sublattice model of the $(Ti)_1(C, N, Va)_{0.5}$ form [40] and the Gibbs energy of the ternary system is thus given by

$$G_m^\alpha = y_{Va}\,{}^\circ G_{Ti}^\alpha + y_C\,{}^\circ G_{TiC_{0.5}}^\alpha + y_N\,{}^\circ G_{TiN_{0.5}}^\alpha + 0.5RT(y_{Va}\ln y_{Va} + y_C \ln y_C + y_N \ln y_N) + y_{Va}y_C\,{}^0L_{C,Va}^\alpha + y_{Va}y_N\,{}^0L_{N,Va}^\alpha + y_C y_N\,{}^0L_{C,N}^\alpha. \quad (2)$$

Here ${}^\circ G_{Ti}^\alpha$ is the Gibbs energy of pure α-Ti, which was adopted from the Scientific Group Thermodata Europe (SGTE) element database [54]. ${}^\circ G_{TiX_{0.5}}^\alpha$ (X is C or N) is the Gibbs energy of a hypothetical hexagonal $TiX_{0.5}$ carbide or nitride. The rudimentary character of this solution model makes it of little interest to use first-principles values for the stability of the $TiX_{0.5}$ carbide or nitride. The calculated values will not correspond to the desired model parameter values, since these are rather dictated by the solution behavior close to pure α-Ti. The temperature dependence of ${}^\circ G_{TiX_{0.5}}^\alpha$ was assumed to be a weighted average of α-Ti and δ-TiC or δ-TiN. A $K_1 + K_2T$ term (K_1 and K_2 are constants) was optimized to reproduce experimental phase boundaries. The interaction parameter was set to zero for carbon (${}^0L_{C,Va}^\alpha$), but optimized for nitrogen (${}^0L_{N,Va}^\alpha$). To keep the model simple we have not used any ternary interaction parameter.

3.2.2. β-Ti

Dissolution of carbon and nitrogen in β-Ti is modeled with a two-sublattice model of the $(Ti)_1(C, N, Va)_3$ form [40]. For the ternary system the Gibbs energy is thus given by

$$G_m^\beta = y_{Va}\,{}^\circ G_{Ti}^\beta + y_C\,{}^\circ G_{TiC_3}^\beta + y_N\,{}^\circ G_{TiN_3}^\beta + 3RT(y_{Va}\ln y_{Va} + y_C \ln y_C + y_N \ln y_N) + y_{Va}y_C\,{}^0L_{C,Va}^\beta + y_{Va}y_N\,{}^0L_{N,Va}^\beta + y_C y_N\,{}^0L_{C,N}^\beta, \quad (3)$$

where ${}^\circ G_{Ti}^\beta$ is the Gibbs energy of pure β-Ti, which was taken from the SGTE element database [54]. Another alternative would be to determine the phase stability (${}^\circ G_{Ti}^\beta$) directly using first-principles calculations, however this value will not describe the properties of β-Ti correctly. This is due to the fact that β-Ti is dynamically unstable at low temperature [57]. The dynamical instability implies that the hypothetical low-temperature β-Ti structure spontaneously transforms into a second structure upon an infinitesimal distortion, which also renders the entropy undefined. By describing this instability in terms of a double-well potential it is possible to work around this problem and reconcile the first-principles predictions with the measured properties at high temperature [58]. Though, this approach will not be applied here. The Gibbs energy of the hypothetical TiX_3 (${}^\circ G_{TiX_3}^\beta$) carbide or nitride was given a sufficiently large value to prevent the BCC phase from appearing at high X concentrations. ${}^\circ G_{TiX_3}^\beta$ was assumed to have a temperature dependence equal to a composition weighted average of the pure elements in their standard states. The interaction parameter ${}^0L_{C,Va}^\beta$ was allowed to vary linearly with temperature and it was optimized to reproduce experimental phase boundaries. A constant interaction parameter ${}^0L_{N,Va}^\beta$ was used in the fitting procedure. The ternary interaction parameter, ${}^0L_{C,N}^\beta$, was set to zero.

3.2.3. The liquid phase

The liquid phase (L) was modeled with a simple substitutional model, in which the Gibbs energy of the ternary system takes the form [40]

$$G_m^{\mathrm{L}} = x_{\mathrm{Ti}} {}^{\circ}G_{\mathrm{Ti}}^{\mathrm{L}} + x_{\mathrm{C}} {}^{\circ}G_{\mathrm{C}}^{\mathrm{L}} + x_{\mathrm{N}} {}^{\circ}G_{\mathrm{N}}^{\mathrm{L}} + RT(x_{\mathrm{Ti}} \ln x_{\mathrm{Ti}} + x_{\mathrm{C}} \ln x_{\mathrm{C}} + x_{\mathrm{N}} \ln x_{\mathrm{N}}) + x_{\mathrm{Ti}}x_{\mathrm{C}} {}^{0}L_{\mathrm{Ti,C}}^{\mathrm{L}} + x_{\mathrm{Ti}}x_{\mathrm{N}}({}^{0}L_{\mathrm{Ti,N}}^{\mathrm{L}} + (x_{\mathrm{N}} - x_{\mathrm{Ti}}) {}^{1}L_{\mathrm{Ti,N}}^{\mathrm{L}}) + x_{\mathrm{Ti}}x_{\mathrm{C}}x_{\mathrm{N}} {}^{0}L_{\mathrm{Ti,C,N}}^{\mathrm{L}}, \quad (4)$$

where x_{Ti}, x_{C} and x_{N} denote the mole fraction of Ti, C and N, respectively. ${}^{\circ}G_{\mathrm{Ti}}^{\mathrm{L}}$, ${}^{\circ}G_{\mathrm{C}}^{\mathrm{L}}$ and ${}^{\circ}G_{\mathrm{N}}^{\mathrm{L}}$ represent the Gibbs energy of liquid Ti, hypothetical liquid nitrogen and hypothetical liquid carbon, respectively. All of these parameters were taken from the SGTE element database [54]. The interaction parameters were fitted to experimentally determined equilibria with the solid and gas phases. The ${}^{1}L_{\mathrm{Ti,X}}^{\mathrm{L}}$ parameter was only used for nitrogen and ${}^{1}L_{\mathrm{Ti,C}}^{\mathrm{L}} = 0$. The ternary interaction parameter ${}^{0}L_{\mathrm{Ti,C,N}}^{\mathrm{L}}$ was not used.

3.2.4. The gas phase

The gas phase was treated as an ideal gas and the following constituent species were included; N_1, N_2, N_3, C_1, C_2, C_3, Ti_1, CN, CNN, NCN, C_2N, C_2N_2, and C_4N_2. All data were taken from the SGTE substance database [59].

3.2.5. The ϵ phase

The ϵ phase (Ti_2X) has the anti-rutile structure [38] and in the binary subsystems it was described as a stoichiometric compound. The temperature dependence was assumed to be a composition weighted average of α-Ti and δ-TiX. First-principles calculations were used to establish the low temperature stabilities. For ϵ-Ti_2N a K_1T term was adjusted to fit the experimentally determined decomposition temperature [37]. The same procedure could not be applied in the carbide case since the ϵ phase is metastable and consequently there is no experimental information. In the ternary system carbon and nitrogen atoms were assumed to mix randomly on the nonmetal sublattice and we did not introduce any interaction parameters.

3.2.6. The graphite phase

Graphite was modeled as pure carbon and the thermodynamic parameters were taken from the SGTE element database [54].

3.2.7. The δ phase

We have tried several different sublattice models for the δ phase. The simplest model contains two sublattices, $(Ti)_1(C, N, Va)_1$, and it is similar to the models used in existing assessments. The expression for the Gibbs energy is

$$G_m^{\delta} = y_{\mathrm{Va}} {}^{\circ}G_{\mathrm{Ti}}^{\delta} + y_{\mathrm{C}} {}^{\circ}G_{\mathrm{TiC}}^{\delta} + y_{\mathrm{N}} {}^{\circ}G_{\mathrm{TiN}}^{\delta} + RT(y_{\mathrm{Va}} \ln y_{\mathrm{Va}} + y_{\mathrm{C}} \ln y_{\mathrm{C}} + y_{\mathrm{N}} \ln y_{\mathrm{N}}) + y_{\mathrm{Va}}y_{\mathrm{C}} {}^{0}L_{\mathrm{C,Va}}^{\delta} + y_{\mathrm{Va}}y_{\mathrm{N}} {}^{0}L_{\mathrm{N,Va}}^{\delta} + y_{\mathrm{C}}y_{\mathrm{N}} {}^{0}L_{\mathrm{C,N}}^{\delta}. \quad (5)$$

${}^{\circ}G_{\mathrm{TiC}}^{\delta}$, ${}^{\circ}G_{\mathrm{TiN}}^{\delta}$ and ${}^{\circ}G_{\mathrm{Ti}}^{\delta}$ are the free energies of δ-TiC, δ-TiN and metastable fcc-Ti. The low temperature enthalpies (298 K) were obtained from first-principles calculations, but the corresponding entropy values were taken from existing assessments [41]. The temperature dependence of ${}^{\circ}G_{\mathrm{Ti}}^{\delta}$ was set equal to that of α-Ti. For ${}^{\circ}G_{\mathrm{TiC}}^{\delta}$ and ${}^{\circ}G_{\mathrm{TiN}}^{\delta}$ we used the temperature dependent parts from the assessment by Frisk et al. [41], which in turn were fitted to the experimental heat content and heat capacities. In the two-sublattice model interaction parameters must be used in order to obtain a realistic thermodynamic description. In the present work the interaction parameters were allowed to depend quadratically on temperature, however a linear dependence would have been sufficient to reproduce the thermodynamic information. The ternary interaction parameter was not used.

The two-sublattice model cannot account for any ordering reactions. In order to capture these phenomena we must formulate a multisublattice model that is consistent with the ordering patterns of TiC_x and TiN_x. In Section 2 we showed that the ordered structures of TiC_x and TiN_x can be described with two different units cells that contain 12 (TiC_x) or 24 (TiN_x) lattice sites. Based on these two unit cells it is possible to derive appropriate sublattice models. For clarity the remaining discussion will be made for the binary Ti-X system (X is C or N), however extension to the ternary case is simply done by allowing carbon, nitrogen and vacancies on each sublattice and modifying the equations accordingly.

The ordered Ti_6X_5, Ti_3X_2 and Ti_2X phases that belong to the $\{111\}_{B1}$ stacking family can be modeled using either three, four or six nonmetal sublattices and one sublattice that only contains Ti atoms. The first model (three nonmetal sublattices) is written as $(Ti)_6(X, Va)_3(X, Va)_2(X, Va)_1$. Each parentheses indicates a separate sublattice and the subscripts denote the number of sites in each sublattice. The first nonmetal sublattice constitutes a full $\{111\}_{B1}$ plane and the last two sublattices together make up the second nonmetal $\{111\}_{B1}$ plane in the unit cell (see Fig. 2). Another possibility is to split also the first nonmetal plane into two sublattices, which yields a model of the $(Ti)_6(X, Va)_2(X, Va)_1(X, Va)_2(X, Va)_1$ form (four nonmetal sublattices). Finally, all nonmetal sites can be treated as separate sublattices, which yields a total of six nonmetal sublattices. This model is written as $(Ti)_6(X, Va)_1(X, Va)_1(X, Va)_1(X, Va)_1(X, Va)_1(X, Va)_1$. The three-, four- and six-sublattice models (here we count only nonmetal sublattices) predict the same ordered structures at low temperature (some exceptions exist for the three-sublattice model), but at finite temperature their predictions differ. The three- and four-sublattice models are not able to predict a completely disordered distribution of elements among sublattices [55], which is a severe drawback since the high temperature disordered phase will then be incorrectly represented. Following Ref. [55], for the two-sublattice model $(A, B)_P(A, B)_Q$ with Gibb's energy defined according to (ideal solid solution)

$$G_m = y_{\mathrm{A}}^{(1)}y_{\mathrm{A}}^{(2)}G_{\mathrm{A:A}} + y_{\mathrm{A}}^{(1)}y_{\mathrm{B}}^{(2)}G_{\mathrm{A:B}} + y_{\mathrm{B}}^{(1)}y_{\mathrm{A}}^{(2)}G_{\mathrm{B:A}} + y_{\mathrm{B}}^{(1)}y_{\mathrm{B}}^{(2)}G_{\mathrm{B:B}} + RTP(y_{\mathrm{A}}^{(1)} \ln y_{\mathrm{A}}^{(1)} + y_{\mathrm{B}}^{(1)} \ln y_{\mathrm{B}}^{(1)}) \quad (6)$$

$$+ RTQ(y_{\mathrm{A}}^{(2)} \ln y_{\mathrm{A}}^{(2)} + y_{\mathrm{B}}^{2} \ln y_{\mathrm{B}}^{(2)}), \quad (7)$$

this property can be shown by realizing that at equilibrium the following equality must be fulfilled;

$$Q\frac{\partial G_m}{\partial y_{\mathrm{A}}^{(1)}} - P\frac{\partial G_m}{\partial y_{\mathrm{A}}^{(2)}} + Q\frac{\partial G_m}{\partial y_{\mathrm{B}}^{(1)}} - P\frac{\partial G_m}{\partial y_{\mathrm{B}}^{(2)}} = x_{\mathrm{B}}(G_{\mathrm{A:B}} - G_{\mathrm{B:A}}) + RT(P - Q) + x_{\mathrm{A}}(G_{\mathrm{B:A}} - G_{\mathrm{A:B}}) + RT(P - Q) = 0. \quad (8)$$

Here we used that for the disordered state $y_{\mathrm{A}}^{(1)} = y_{\mathrm{A}}^{(2)} = x_{\mathrm{A}}$ and $y_{\mathrm{B}}^{(1)} = y_{\mathrm{B}}^{(2)} = x_{\mathrm{B}}$. The last equility follows from $\frac{\partial G_m}{\partial y_{\mathrm{A}}^{(1)}} = \frac{\partial G_m}{\partial y_{\mathrm{A}}^{(2)}} = \frac{\partial G_m}{\partial y_{\mathrm{B}}^{(1)}} = \frac{\partial G_m}{\partial y_{\mathrm{B}}^{(2)}} = 0$ at equilibrium and, apart from special cases, this can only be fulfilled if $P = Q$ and $G_{\mathrm{A:B}} = G_{\mathrm{B:A}}$, i.e. if sublattice (1) and (2) contain the same number of sites and are equivalent. The reasoning above can be extended to any number of sublattices. It is possible to correct for this deficiency by adding interaction parameters of Redlich–Kister form that force the minimum to occur for the disordered site distribution at sufficiently high temperature [55]. Due to the multisublattice character of our models this solution turns out to be impractical. The six-sublattice model has the same number of sites in each sublattice, which, at sufficiently high temperature, results in a minimum Gibbs energy

Table 3
The compound column lists all the end-member compounds in the six-sublattice models for a hypothetical A–B system

Compound	α_1^{A-B} ($\boldsymbol{R}_1$) $\boldsymbol{R}_1 = \frac{a}{2}\langle 110\rangle$	α_2^{A-B} ($\boldsymbol{R}_2$) $\boldsymbol{R}_2 = a\langle 100\rangle$	α_3^{A-B} ($\boldsymbol{R}_4$) $\boldsymbol{R}_3 = \frac{a}{2}\langle 112\rangle$	α_4^{A-B} ($\boldsymbol{R}_5$) $\boldsymbol{R}_4 = a\langle 110\rangle$	α_5^{A-B} ($\boldsymbol{R}_6$) $\boldsymbol{R}_5 = \frac{a}{2}\langle 130\rangle$
AAAAAA	0; 0	0; 0	0; 0	0; 0	0; 0
AAAAAB, AAAABA, AAABAA, AABAAA, AABAAA, BAAAAA	−0.2; −0.2	−0.2; −0.2	0.2; 0.2	0; 0	0; 0
AAAABB, AAABAB, AAABBA, BBAAAA, BABAAA, ABBAAA	−0.125; −0.25	−0.5; 0	0.125; 0.25	0.375; −0.1250	0; −0.1250
BAABAA, ABAABA, AABAAB	−0.25; −0.25	0; 0	0.25; 0.25	−0.25; −0.25	0; 0
BAAABA, BAAAAB, ABABAA, ABAAAB, AABBAA, AABABA	−0.25; −0.125	0; −0.5	0.25; 0.125	−0.25; 0.25	0; 0.125
AAABBB, BBBAAA	0; −1/3	−1; 1/3	0; 1/3	1; −1/3	0; −1/3
AABBBA, ABABAB, BAAABB, BBAAAB, BABABA, ABBBAA	−2/9; −1/9	−1/9; −5/9	2/9; 1/9	−1/9; 3/9	0; 1/9
AABABB, AABBAB, ABAABB, ABABBA, BAABAB, BAABBA, BBAABA, BBABAA, BABBAA, BABAAB, ABBABA, ABBAAB	−2/9; −2/9	−1/9; −1/9	2/9; 2/9	−1/9; −1/9	0; 0
ABBBAB, ABBBBA, BABABB, BABBBA, BBAABB, BBABAB	−0.25; −0.125	0; −0.5	0.25; 0.125	−0.25; 0.25	0; 0.125
ABBABB, BABBAB, BBABBA	−0.25; −0.25	0; 0	0.25; 0.25	−0.25; −0.25	0; 0
BBBBAA, BBBABA, BBBAAB, AABBBB, ABABBB, BAABBB	−0.125; −0.25	−0.5; 0	0.125; 0.25	0.375; −0.125	0; −0.125
BBBBBA, BBBBAB, BBBABB, BBABBB, BBABBB, ABBBBB	−0.2; −0.2	−0.2; −0.2	0.2; 0.2	0; 0	0; 0
BBBBBB	0; 0	0; 0	0; 0	0; 0	0; 0

A–B corresponds to X–Va in the $(Ti)_6(X, Va)_1(X, Va)_1(X, Va)_1(X, Va)_1(X, Va)_1(X, Va)_1$ model and the table notation omits the Ti sublattice. The compounds that are grouped together are equivalent. The notation is the same for the $\{111\}_{B1}$ and $\{011\}_{B1}$ stacking models. The remaining columns show the A–B effective Warren–Cowley SRO parameters up to the fifth coordination shell (see text). The vector $\boldsymbol{R}_i$ ($i = 1, 2, 3, 4, 5$) represents the site separation for coordination shell i. The values for the $\{111\}_{B1}$ stacking and the $\{011\}_{B1}$ stacking are separated by '; '.

for the disordered site distribution. Another consequence of the incomplete symmetry properties of the three- and four-sublattice models is that, compared to the six-sublattice model and the Monte-Carlo simulations in Ref. [22], they predict an incorrect topology for the ordering reactions in δ-TiC_x. All together, neither the three- nor the four-sublattice model is capable of representing the true physical properties of TiC_x and for that reason we prefer to work with the six-sublattice model, even though this choice introduces some additional complexity. For example, the number of end-member compounds will be significantly higher than for the three- and four-sublattice models. The crystallographic view of the six-sublattice division is specified in Table 1 and illustrated in Fig. 2. Table 3 lists all the end-member compounds in the six-sublattice model and summarizes their X–Va correlation properties (see Section 4.3.1 for further discussion). The CEF expression for the Gibbs energy in the six-sublattice model is

$$\begin{aligned} G_m^{\delta} = {} & \sum y_i^{(1)} y_j^{(2)} y_k^{(3)} y_l^{(4)} y_m^{(5)} y_n^{(6)} \circ G_{Ti:i:j:k:l:m:n} \\ & + RT\left(\sum y_i^{(1)} \ln y_i^{(1)} + \sum y_j^{(2)} \ln y_j^{(2)}\right. \\ & + \sum y_k^{(3)} \ln y_k^{(3)} + \sum y_l^{(4)} \ln y_l^{(4)} \\ & \left. + \sum y_m^{(5)} \ln y_m^{(5)} + \sum y_n^{(6)} \ln y_n^{(6)}\right) + {}^{E}G_m . \end{aligned} \tag{9}$$

Here ${}^{\circ}G_{Ti:i:j:k:l:m:n}$ is the free energy of the $(Ti)_6(i)_1(j)_1(k)_1(l)_1(m)_1(n)_1$ (i, j, k, l, m, n = X or Va) end-member compound and $y_i^{(1)}$ is the site fraction of component i in sublattice 1, etc. The first sum covers all end-member compounds and the remaining sums cover all sublattice constituents.

The Ti_6X_5, Ti_3X_2 and Ti_2X compounds that order according to the $\{011\}_{B1}$ stacking pattern can be described by dividing the nonmetal sublattice in the 24-site unit cell (Fig. 4) into four or six separate sublattices. We prefer the six-sublattice division, since only this model fulfill the symmetry conditions (equal number of sites in all the nonmetal sublattices) that are required in order to predict the correct phase diagram topology. In the $\{011\}_{B1}$ six-sublattice model, which is represented as $(Ti)_{12}(X, Va)_2(X, Va)_2(X, Va)_2(X, Va)_2(X, Va)_2(X, Va)_2$, all the $\{011\}_{B1}$ planes are split into two different sublattices. Each of these two sublattices are then joined with the corresponding sites on the third nearest neighbor $\{011\}_{B1}$ plane to form one common sublattice. In total the 24-site unit cell contains six $\{011\}_{B1}$ planes. This situation is illustrated in Fig. 4 and the sublattice division is specified in Table 2. All the end-member compounds in the $\{011\}_{B1}$ six-sublattice model are listed in Table 3 together with their X–Va correlation properties. The expression for the Gibbs free energy of the $\{011\}_{B1}$ model is equivalent to Eq. (9), but with a factor of 2 in front of the configurational entropy terms, which accounts for the sublattice multiplicity. It would be virtually impossible to estimate all the end-member energies in the $\{111\}_{B1}$ and $\{011\}_{B1}$ multisublattice models from experimental data; however first-principles calculations give us access to the properties of the ordered compounds at low temperature (the enthalpies at 0 K). In order to predict thermodynamic properties at finite temperature we also need to know the free energy as function temperature. In the following discussion we refer to the phonon and electronic contributions to the free energy, since the contributions from the configurational energy and entropy are modeled with the site fraction expansion in Eq. (9). For pure compounds and certain stoichiometric phases, e.g. α-Ti and δ-TiC, the thermal properties are often well known from experiments. Conversely, the thermal properties of for example nonstoichiometric titanium nitride (TiN_x) are not known from experiments. For our purpose this implies that the temperature dependence of the end-member energies (${}^{\circ}G_{Ti:i:j:k:l:m:n}$) is unknown for the vacancy-containing compounds. However, as a good approximation one may estimate the temperature dependence as a composition weighted average of

the temperature dependence of ${}^{\circ}G^{\delta}_{\mathrm{Ti}}$ and ${}^{\circ}G^{\delta}_{\mathrm{TiX}}$, which are known from experiments (we recall that the temperature dependence of ${}^{\circ}G^{\delta}_{\mathrm{Ti}}$ is assumed to be equal to the temperature dependent part of ${}^{\circ}G^{\alpha}_{\mathrm{Ti}}$). This procedure is equivalent to the so-called Neumann–Kopp rule [60] and, unless otherwise stated, we will use this approach. The thermal contribution to the free energy from lattice vibrations can also be estimated by calculating the phonon spectra for each nonstoichiometric compound using first-principles calculations, as was recently done for a range of stoichiometric transition metal carbides and nitrides [61]. This will provide an estimate for the deviation from the Neumann–Kopp rule. Because of the huge time consumption of such calculations, they are presently deemed impractical. Instead we prefer to use a simpler approach, based on the Debye–Grüneisen model [60], to calculate the phonon contribution the temperature dependence of the compound energies. We are primarily interested in estimating not the absolute values, but rather the deviation from the Neumann–Kopp rule. The reason for this is that we do not want to alter the well-established thermal properties of α-Ti, δ-TiC and δ-TiN. Additionally, the Debye–Grüneisen model is more accurate for studying systematic deviations from the reference state (the Neumann–Kopp rule) than the absolute thermal properties of the δ phase compounds. Recently Lu et al. discussed the application of a Debye–Grüneisen model to pure elements [62] as well as to binary carbides and nitrides [63]. In the Debye–Grüneisen model the expressions for the vibrational energy (E_D) and entropy (S_D) are [60]

$$E_D(T,V) = \frac{9}{8}Nk_B\theta_D + 3Nk_BTD\left(\frac{\theta_D}{T}\right) \tag{10}$$

and

$$S_D(T,V) = 3Nk_B\left(\frac{4}{3}D\left(\frac{\theta_D}{T}\right) - \ln\left(1-\exp-\frac{\theta_D}{T}\right)\right). \tag{11}$$

Here N is the number of atoms, k_B is the Boltzmann constant, $\theta_D(V)$ denotes the Debye temperature and D the Debye function. In order to evaluate Eqs. (10) and (11) the Debye temperature as well as its volume dependence (anharmonic contribution to the lattice vibrations) must be known. According to Ref. [63] the Dugdale–MacDonald (DM) [64] expression for the volume dependence of $\theta_D(V)$, i.e. the Grüneisen parameter, gives reasonable results for most carbides and nitrides, and consequently we adopt this model. The DM expression [64] for $\theta_D(V)$ of TiX_x reads [63]

$$\theta_D(V) = k(\nu)\frac{\hbar}{k_B\sqrt{rm}}(6\pi^2 rN_A)^{\frac{1}{3}}V^{\frac{2}{3}}\left(-\frac{\partial P(V)}{\partial V} - \frac{2}{3}\frac{P}{V}\right)^{\frac{1}{2}}, \tag{12}$$

where $r = 1 + x_X/(1-x_X)$, N_A is Avogadro's number, V is volume per mole TiX_x and $\hbar$ is the Planck constant (over 2π). The factor r accounts for the variable stoichiometry of TiX_x. The mass m is an effective atomic mass defined as the logarithmic average of all the masses in the formula unit. Finally, $k(\nu)$, which depends on the Poisson ratio ν, is given by

$$k(\nu) = \left(\frac{2}{3}\left(\frac{2(1+\nu)}{3(1-2\nu)}\right)^{\frac{3}{2}} + \frac{1}{3}\left(\frac{1+\nu}{3(1-\nu)}\right)^{\frac{3}{2}}\right)^{-\frac{1}{3}}. \tag{13}$$

Lu et al. [63] used ν as fitting parameter to reproduce experimental Debye temperatures, but ν can also be calculated from theoretical models of the elastic material properties, see for example Ref. [65]. In the present work we make the simplifying assumption that ν varies linearly with the composition between the Ti and TiX end points. Our results and conclusions do not critically depend on this choice. The Poisson ratio of α-Ti was taken from experiments, while we used the fitted values due to Lu et al. [63] for δ-TiX (these are in good agreement with experiments). In order to evaluate Eq. (12) the pressure–volume relation must be established. For this purpose we applied the Murnaghan equation of state [50], which was fitted to the calculated energy–volume curve. The total Gibbs energy is

$$G(T,V) = E(V) + E_D(T,V) - TS_D(T,V). \tag{14}$$

$E(V)$ is the 0 K total energy, including the volume dependence according to the Murnaghan equation of state. The contributions due to thermal electronic excitations, $E_{el}(T,V)$ and $S_{el}(T,V)$, are assumed to be small and it is therefore neglected in Eq. (14). The equilibrium volume for each temperature is determined by minimizing the Helmholtz Free energy and this volume is then used for evaluating the Gibbs free energy according to Eq. (14). Finally, the deviation from the Neumann–Kopp rule is estimated by calculating the difference between $G(T,V)$ for a particular compound and the composition weighted average of $G(T,V)$ for δ-Ti and δ-TiX.

4. Results and discussion

4.1. Thermodynamic properties of the end-member compounds

4.1.1. Titanium carbide, TiC_x

Fig. 6 shows the calculated formation energies (H_f) of the $\{111\}_{B1}$ TiC_x end-member compounds. The analogous formation energies, but expressed with respect to fcc-Ti and δ-TiC, are plotted in the inset. There are several data points for each composition, which follows from the fact that a particular composition can be realized by filling different sublattices with carbon atoms. We confirm the stability of the vacancy ordered Ti_6C_5 ($AAAAAB_{\{111\}}$), Ti_3C_2 ($AAAABB_{\{111\}}$) and Ti_2C ($AAABBB_{\{111\}}$) structures and we predict a minimum formation energy at the Ti_6C_5 composition. For the most stable Ti_6C_5, Ti_3C_2 and Ti_2C compounds every second nonmetal $\{111\}_{B1}$ plane is completely filled with carbon atoms, while the other nonmetal plane is either empty (Ti_2C) or partially filled (Ti_3C_2 and Ti_6C_5). Fig. 6 also includes the formation energy of cubic Ti_2C, which is slightly lower in energy than the trigonal form [34] described by our sublattice model. For stoichiometric TiC our calculated value agrees with experiments [27,66–68] within the expected error limits. The experimental data for nonstoichiometric TiC_x [27,66–74] are widely spread and our theoretical predictions lie within the same range. In accordance with carbon activity data for TiC_x [27,75] our calculations predict a minimum formation energy at the Ti_6C_5 composition. The existence of this minimum is not immediately obvious from experimental formation energies alone [27]. Since δ-TiC_x is metastable with respect to α-Ti + δ-TiC_x for $x_C < 0.375$ ($x < 0.6$) it is not possible to investigate this range experimentally. The curvature of the stability line in the inset of Fig. 6 indicates that the δ phase has a miscibility gap for $x_C < 1/3$ ($x < 0.5$).

In Fig. 7 we compare the electronic density of states (DOS) for Ti_6C_5 ($AAAAAB_{\{111\}}$) and for vacancy-free TiC. Clearly both compounds are metallic and the maximum stability of Ti_6C_5 is related to filling of the vacancy induced states just below the Fermi level. The projected density of states reveals that these states (narrow peaks in the vicinity of the Fermi level ± 1 eV) are due to an increased C-2p–Ti-3d hybridization, which counteracts the energy cost of breaking bonds upon removal of C from TiC [76]. The stability of the Ti_2C structure with empty lattice planes is related to the formation of a gap within the C-2p–Ti-3d band and a minimum DOS close to the Fermi level (see dotted line in Fig. 8). These features are not present for the other Ti_2C structures, whose DOS are also plotted in Fig. 8. The C-2p–Ti-3d gap separates the lower part of the band that consists of hybridized p–d states and the upper part of mainly Ti-3d character. The gap originates from

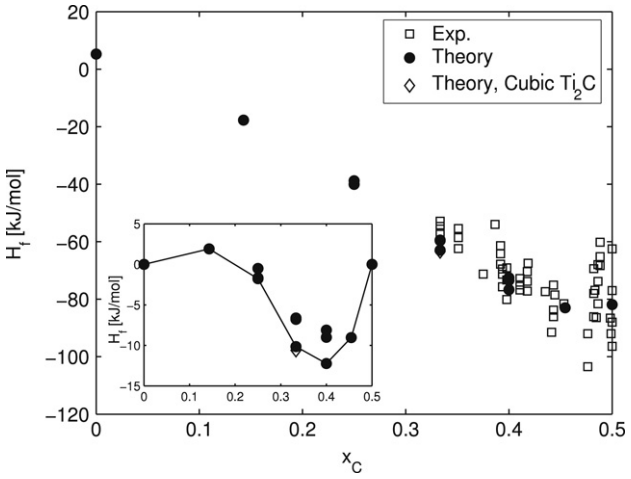

Fig. 6. The formation energy (H_f) of the $\{111\}_{B1}$ TiC_x end-member compounds at 0 K. The cubic form of Ti_2C is also included. The experimental data were taken from Frisk et al. [27] and references therein (see Fig. 2 in Ref. [27]). The experimental data refers to 298 K. The inset shows the corresponding formation energies expressed with respect to fcc-Ti and δ-TiC. The solid line connects the lowest-energy structures. From low to high carbon concentration these structures are $AAAAAA_{\{111\}}$, $AAAAAB_{\{111\}}$, $AABAAB_{\{111\}}$, $AAABBB_{\{111\}}$, $AABBBB_{\{111\}}$, $ABBBBB_{\{111\}}$ and $BBBBBB_{\{111\}}$.

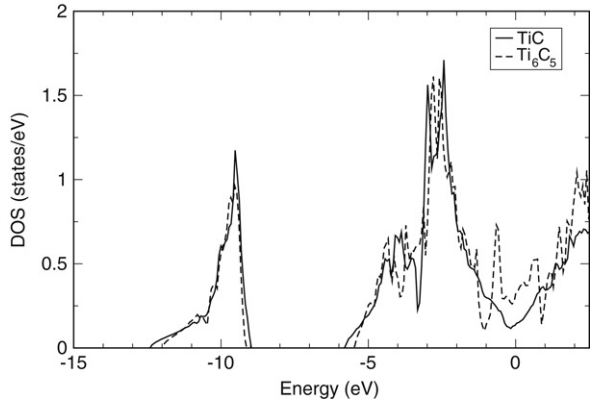

Fig. 7. The DOS of Ti_6C_5 and TiC. The Fermi level is at 0 eV.

the absence of p–d bonds within and across the empty $\{111\}_{B1}$ planes.

In Fig. 9 we compare the stability of TiC_x in the $\{011\}_{B1}$ stacking model with the most stable $\{111\}_{B1}$ structures. For the Ti_2C composition the ground state $\{111\}_{B1}$ structure is undoubtedly more stable than the corresponding $\{011\}_{B1}$ structures, but for other compositions the energy difference between the lowest-energy structures in the two stacking models is quite small. The degeneracy for compositions away from Ti_2C can be rationalized in terms similar carbon-vacancy correlation functions (see Table 3). The $\{011\}_{B1}$ and $\{111\}_{B1}$ models are identical at the Ti and TiC ends.

The calculated molar volumes (V_m) of the $\{111\}_{B1}TiC_x$ end-member compounds are plotted in Fig. 10. Compared to experiments [30,77–79] the molar volume is overestimated by approximately 1%, a typical systematic error of DFT calculations employing the generalized gradient approximation. V_m depends on the exact configuration of carbon vacancies, i.e. two end-members with the same carbon composition have different molar volume. For each composition the molar volume of the most stable end-member compound is highlighted in Fig. 10. Except for the Ti_6C_2 composition the smallest molar volume is associated with the most stable end-member compound. The most stable Ti_2C structure, with one completely empty $\{111\}_{B1}$ lattice plane ($AAABBB_{\{111\}}$), has a molar volume that is significantly lower than the molar

Fig. 8. The DOS of Ti_2C in the $AAABBB_{\{011\}}$, ϵ-Ti_2N and $AAABBB_{\{111\}}$ structure types. The Fermi level is at 0 eV.

Fig. 9. The formation energy (H_f) of the $\{011\}_{B1}$ TiC_x end-member compounds at 0 K. The lowest-energy $\{111\}_{B1}$ compounds are also included.

Fig. 10. The molar volume (V_m) of the $\{111\}_{B1}$ TiC_x end-member compounds at 0 K. For each composition the volume of the most stable structure is plotted with black solid dots (compare Fig. 6). Experimental values from Refs. [77] (Ramqvist), [78] (Bittner et al.), [79] (Fernandes et al.) and [30] (Moisy-Maurice et al.) are also included. Unless otherwise noted the experimental data refers to 298 K.

volume for the structures with carbon atoms spread over all the $\{111\}_{B1}$ planes. The ground-state Ti_6C_2 compound does not have any empty lattice planes, but some of the metastable compounds do, which explains why it does not correspond to the smallest V_m.